Text S1

We assume that linear elastic theory holds for small lattice strains experienced due to deviatoric stress (e.g., Singh and Balasingh 1993, 1994; Singh et al. 1998). For a sample deformed under axial compression, the stress state is described by the following:

$$\sigma_{ij} = \begin{bmatrix} \sigma_1 & 0 & 0 \\ 0 & \sigma_1 & 0 \\ 0 & 0 & \sigma_3 \end{bmatrix} = \begin{bmatrix} \sigma_P & 0 & 0 \\ 0 & \sigma_P & 0 \\ 0 & 0 & \sigma_P \end{bmatrix} + \begin{bmatrix} -t/3 & 0 & 0 \\ 0 & -t/3 & 0 \\ 0 & 0 & 2t/3 \end{bmatrix}$$

$$= \sigma_P + D_{ij}$$

Where σ_{ij} is the stress state of the sample, σ_P is the hydrostatic stress component, t is the axial stress component, and D_{ij} is the deviatoric stress. As we probe the sample perpendicular to the compression direction, we are able to measure variations in lattice spacing with respect to the compression direction, i.e. the lattice strain.
For the radial diffraction geometry, diffraction patterns have variations in d-spacing and intensities with azimuth. The measured d-spacings (d_m) are fit using a hydrostatic component (d_P) and the angle between the diffraction plane normal and the compression axis (χ):

$$d_m(hkl, \chi) = d_P(hkl)[1 + Q(hkl)(1 - 3\cos^2 \chi)]$$

From this, we fit a value for Q that is a measure of the elastic strain on an individual lattice plane. Systematic intensity variations around Debye rings are due to texture.

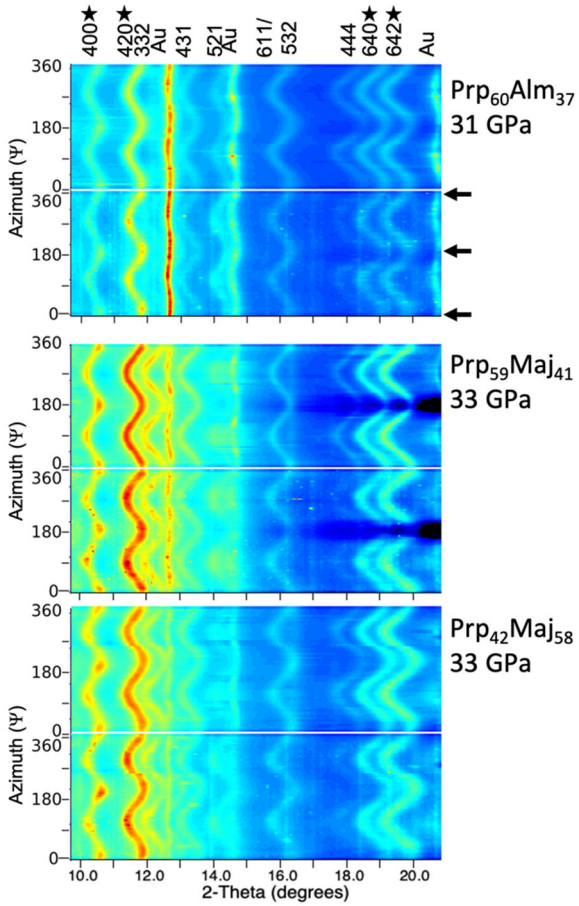

Figure S1. Representative unrolled diffraction images of $Prp_{60}Alm_{37}$, $Prp_{59}Maj_{41}$, and $Prp_{42}Maj_{58}$ with gold at 31 or 32 GPa; calculated diffraction patterns are on top, and experimental diffraction patterns on the bottom of each panel. The compression direction is indicated by arrows. Stars indicate those diffraction lines that were used to calculate strength and compared with modeling results.

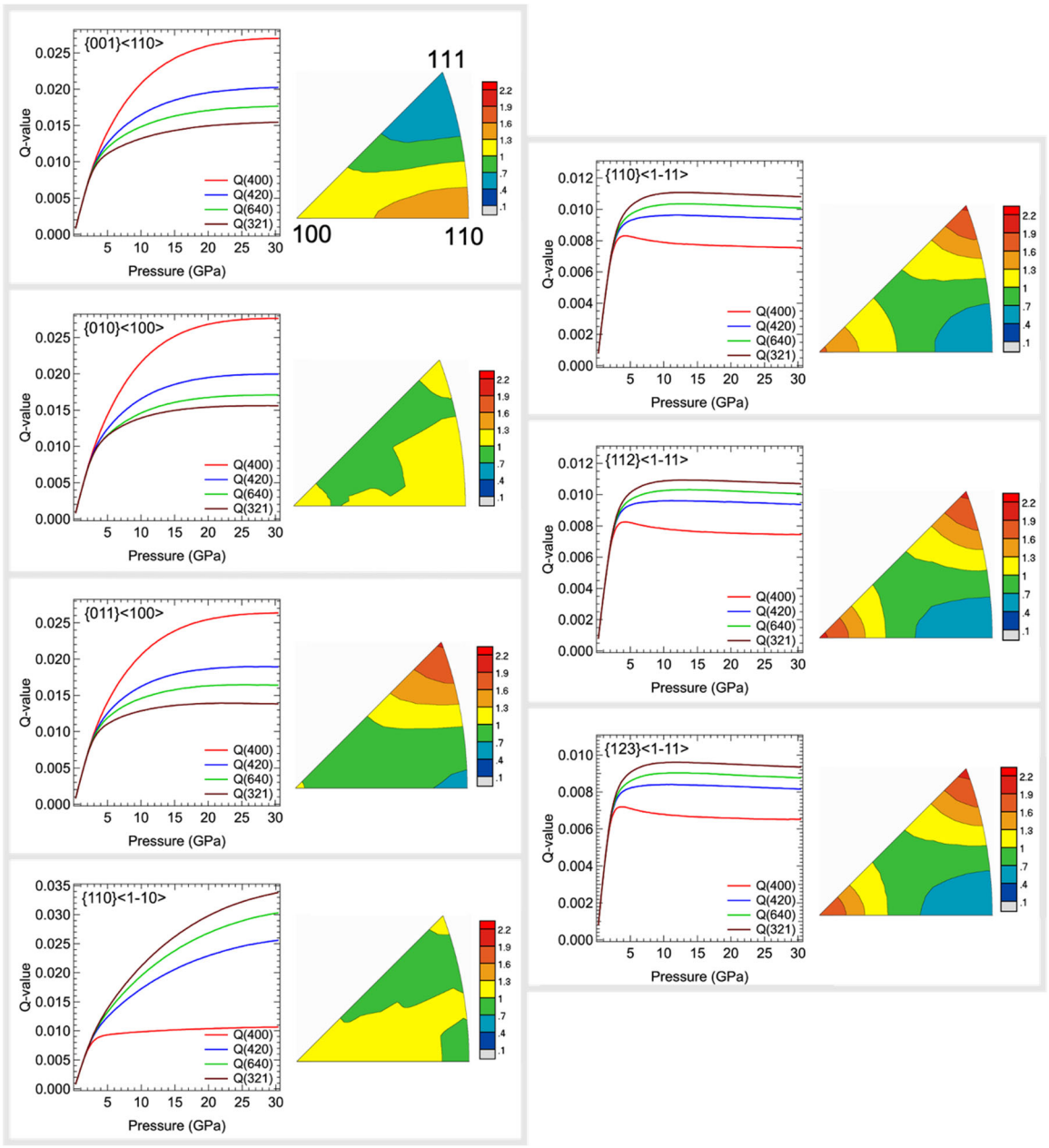

Figure S2. Single slip systems tested for garnet with the resulting *Q*-factors and texture development, as shown with inverse pole figures, up to 30 GPa.

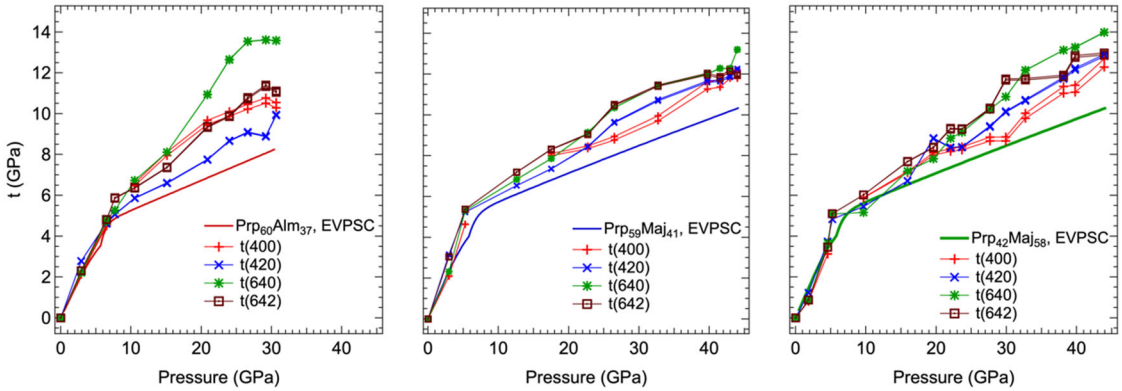

Figure S3. Modeled vs experimental strength (for each of the four diffraction lines (400), (420), (640), and (642)) for (left) $Prp_{60}Alm_{37}$, (middle) $Prp_{59}Maj_{41}$, (right) $Prp_{42}Maj_{58}$.

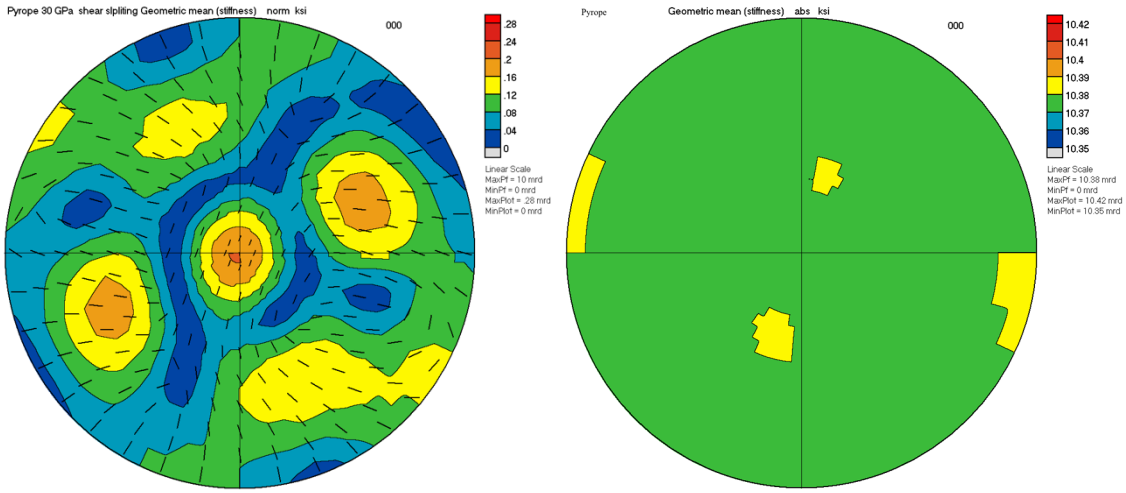

Figure S4. (left) Shear wave splitting of pyrope and (right) p-wave velocity of a pyrope aggregate at 30 GPa.

Table S1. Parameters used for EVPSC modeling.

Slip System	τ_0	$d\tau/dP$	$d^2\tau/dP^2$	n
$Prp_{60}Alm_{37}$				
{110}<1-11>	3.2	0.12	0.0	5
{001}<110>	3.0	0.12	0.0	5
$Prp_{59}Maj_{41}$				
{110}<1-11>	3.7	0.12	-0.00015	5
{001}<110>	3.5	0.12	-0.00015	5
$Prp_{42}Maj_{58}$				
{110}<1-11>	3.65	0.12	-0.00015	5
{001}<110>	3.45	0.12	-0.00015	5

Table S2. Calculated strength with pressure using $t = 6G < Q(hkl) >$; used diffraction lines: (400), (420), (640), and (642). *G = 94.7 GPa (Chai et al., 1997), dG/dP=1.76, ** G = 90 GPa (Sinogeikin & Bass, 2002), dG/dP=1.3

$Prp_{60}Alm_{37}$*			$Prp_{59}Maj_{41}$**			$Prp_{42}Maj_{58}$**		
Pressure (GPa)	Experiment t (GPa)	EVPSC t (GPa)	Pressure (GPa)	Experiment t (GPa)	EVPSC t (GPa)	Pressure (GPa)	Experiment t (GPa)	EVPSC t (GPa)
0.0	0	0	0.0	0.00	0	0.0	0.00	0
2.9	2.31	1.93	3.0	2.56	2.35	1.8	0.91	1.34
6.5	4.67	4.43	5.3	4.98	3.81	4.6	3.38	3.28
6.5	4.77	4.43	12.6	6.72	6.10	5.2	4.80	3.79
7.7	5.25	4.85	17.5	7.78	6.79	9.7	5.49	5.63
10.5	6.13	5.32	22.7	8.69	7.53	15.9	7.05	6.54
15.1	7.13	6.02	26.5	9.78	8.01	19.6	8.14	7.02
20.9	8.83	6.87	32.7	10.86	8.85	22.1	8.57	7.37
24.0	9.60	7.31	39.7	11.85	9.77	23.7	8.68	7.57
26.6	10.32	7.68	41.5	11.92	10.02	27.6	9.61	8.11
29.2	10.62	8.06	42.9	12.19	10.15	29.9	10.31	8.44
30.7	10.75	8.26	44.0	12.46	10.35	32.7	11.09	8.79
						38.1	12.02	9.52
						39.8	12.44	9.71
						43.9	13.18	10.22

References

Chai, M., Brown, J. M., & Slutsky, L. J. (1997). The elastic constants of a pyrope-grossular-almandine garnet to 20 GPa. *Geophysical Research Letters*, *24*(5), 523. https://doi.org/10.1029/97GL00371

Singh, A. K., & Balasingh, C. (1993). The lattice strains in a specimen (cubic system) compressed nonhydrostatically in an opposed anvil high pressure setup. *Journal of Applied Physics*, *73*, 4278–4286. https://doi.org/10.1063/1.355786

Singh, A. K., & Balasingh, C. (1994). The lattice strains in a specimen (hexagonal system) compressed nonhydrostatically in an opposed anvil high pressure setup. *Journal of Applied Physics*, *75*(10), 4956–4962. https://doi.org/10.1063/1.355786

Singh, A. K., Balasingh, C., Mao, H., Hemley, R. J., & Shu, J. (1998). Analysis of lattice strain measured under nonhydrostatic pressure. *Journal of Applied Physics*, *83*(12), 7567–7575.

Sinogeikin, S. V, & Bass, J. D. (2002). Elasticity of majorite and a majorite-pyrope solid solution to high pressure: Implications for the transition zone. *Geophysical Research Letters*, *29*(2), 1017. https://doi.org/10.1029/2001GL013937